Quasi-free $(\alpha,2\alpha)$ reaction induced by 140 MeV alpha particles on ^{9}Be, ^{12}C, ^{16}O, and ^{20}Ne

C. W. Wang,* N. S. Chant, P. G. Roos, A. Nadasen, and T. A. Carey
Department of Physics and Astronomy, University of Maryland, College Park, Maryland 20742
(Received 26 November 1979)

Measurements of the $(\alpha,2\alpha)$ reaction on ^{9}Be, ^{12}C, ^{16}O, and ^{20}Ne targets at $E_\alpha = 140$ MeV were made at 20 angle pairs. The quasi-free knockout mechanism appears to dominate the reaction. The experimental data were analyzed with distorted-wave impulse approximation calculations. The factorization approximation employed in the calculations was tested explicitly and found to be valid. The shapes of the calculated energy sharing spectra are in satisfactory agreement with the data. The predicted absolute cross sections were found to be very sensitive to the cluster-core bound state radius parameter, and a bound state radius $R = 2.52A_c^{1/3}$ fm is necessary to obtain absolute spectroscopic factors consistent with existing theoretical values. Several possible explanations for this excessive value are suggested. Comparisons are made with other alpha knockout and transfer reactions.

[NUCLEAR REACTIONS ^{9}Be, ^{12}C, ^{16}O, ^{20}Ne $(\alpha,2\alpha)$, $E_\alpha = 140$ MeV; measured $\sigma(E_{\alpha1}, E_{\alpha2}, \theta_{\alpha1}, \theta_{\alpha2})$ DWIA analysis; deduced absolute spectroscopic factors.]

I. INTRODUCTION

Quasi-free knockout reactions have proved to be a powerful tool for the investigation of nuclear structure. Since the first experiment studying $(p,2p)$ reactions on light nuclei,[1] a considerable amount of experimental and theoretical work has been carried out on this subject. In situations where the quasi-free knockout reaction mechanism dominates, the $(p,2p)$ reaction can provide two types of information.[1-6] Firstly, the proton hole states in nuclei can be investigated, and secondly, one can study off-energy-shell p-p interactions. Similar information about nucleon clusters in nuclei can be obtained using quasi-free cluster knockout reactions.[4]

In this paper we present studies of alpha clustering using the $(\alpha,2\alpha)$ reaction at 140 MeV. In recent years alpha clustering in $1p$ and $2s1d$ shell nuclei has been studied using a variety of nuclear reactions. The $(d,^{6}\mathrm{Li})$, $(^{3}\mathrm{He},^{7}\mathrm{Be})$, $(\alpha,^{8}\mathrm{Be})$, $(^{6}\mathrm{Li},d)$, $(^{7}\mathrm{Li},t)$, and $(^{16}\mathrm{O},^{12}\mathrm{C})$ alpha transfer reactions[7-13] has been studied and analyzed using distorted wave Born approximation (DWBA) and coupled channel Born approximation (CCBA) calculations.[14] However, most of these analyses are limited to extracting relative alpha spectroscopic factors. The $(p,p\alpha)$ quasi-free knockout reaction has been investigated in several works.[15-18] Analyses of the experimental results at an incident energy of 100 MeV have shown that the plane wave impulse approximation (PWIA) reaction model is inadequate but that the data are well described by distorted wave impulse approximation (DWIA) calculations.[19-21] In these analyses the extracted *absolute* alpha cluster spectroscopic factors are found to be in good agreement with theoretical calculations.[22,23]

The $(\alpha,2\alpha)$ quasi-free knockout reaction on $1p$ and $2s1d$ shell nuclei has also been studied by other groups. Results for the $^{6,7}\mathrm{Li}(\alpha,2\alpha)$ reaction at $E_\alpha = 50$ to 80 MeV (Refs. 24 and 25) have been analyzed using the PWIA. Also a reaction mechanism study of $^{9}\mathrm{Be}(\alpha,2\alpha)$ at $E_\alpha = 40$ to 60 MeV has been reported.[26,27] In addition, data have been obtained for the $^{20}\mathrm{Ne}(\alpha,2\alpha)$ reaction at $E_\alpha = 78$ MeV (Ref. 28) and analyzed using the PWIA. Recently, Sherman *et al.*[29,30] have carried out extensive measurements of the $(\alpha,2\alpha)$ reaction on nine nuclei from ^{12}C to ^{66}Zn at $E_\alpha = 90$ MeV. Finally the ^{16}O, $^{28}\mathrm{Si}(\alpha,2\alpha)$ reactions have been studied at 0.65 and 0.85 GeV.[31]

The most complete $(\alpha,2\alpha)$ study is the work of Sherman *et al.*, at 90 MeV which poses some interesting problems. Using an approximate parametrized form for the distorted waves[32] quite good agreement was obtained with the shape of the energy sharing spectra and the results were insensitive to the type of bound state wave function used. The alpha spectroscopic factors obtained from this analysis are 2.9 ± 0.4 and 2.9 ± 0.5 for $^{12}\mathrm{C}[\alpha + ^{8}\mathrm{Be}(\mathrm{g.s.})]$ and $^{16}\mathrm{O}[\alpha + ^{12}\mathrm{C}(\mathrm{g.s.})]$, respectively, which should be compared to the theoretical values of 0.55 and 0.23 obtained by Kurath.[22] However, for the $^{16}\mathrm{O}(\alpha,2\alpha)^{12}\mathrm{C}$ data of Sherman *et al.*, calculations by Chant and Roos,[19] using an exact partial wave expansion of the distorted waves and a Woods-Saxon bound state wave function with parameters chosen to reproduce the rms radius of ^{16}O, yield absolute spectroscopic factors roughly 100 times the theoretical prediction. In spite of this unexpected result, the ratio S_{0^+}/S_{2^+} of

the spectroscopic factors for ^{12}C(g.s.) and the first excited state of ^{12}C(4.43 MeV, 2$^+$) was found to be $\frac{1}{8}$, fairly close to the value 1/5.7 of Kurath. At $E_\alpha = 850$ MeV, Chant and Roos obtained a value of 1.8 for S_α which is an upper limit since many levels contributed due to poor binding energy resolution of the experiment.[31]

Studies[33,34] of ^{16}O$(\alpha, 2\alpha)^{12}$C(g.s.) at $E_\alpha = 25$ MeV and ^{16}O, ^{20}Ne$(p, p\alpha)$ at $E_p = 46.8$ MeV showed that the alpha removal reaction at these energies is dominated by sequential processes, while in the systematic study of Sherman *et al.*,[29,30] at $E_\alpha = 90$ MeV the quasi-free knockout mechanism appeared to dominate. Nevertheless, since the difficulties in Sherman's approximate DWIA analysis and in the exact DWIA treatment of Chant and Roos may arise from the presence of competing processes at this energy, we chose to study the $(\alpha, 2\alpha)$ reaction at a higher energy, $E_\alpha = 140$ MeV, in the hope that the reaction mechanism might be more easily understood and hence more reliable nuclear structure information obtained. Results for ^{9}Be, ^{12}C, ^{16}O, and ^{20}Ne targets are presented. The experimental details and results are presented in Sec. II. A DWIA analysis of the data is presented in Sec. III. An important feature of this section is a series of explicit tests of the factorization approximation employed in the analysis which serve to establish the validity of the assumed reaction mechanism. As a prerequisite to a comparison of experimental and theoretical values for the alpha cluster spectroscopic factors it is important to be aware of the sensitivity of the results to the various parameters associated with the DWIA calculations. Thus, in Sec. III we also present studies of these sensitivities together with comparison of our results with theoretical predictions and the other experimental studies. Finally the implications of our results are discussed in Sec. IV.

II. EXPERIMENT

A. General description

A 140 MeV alpha beam from the University of Maryland sector-focused isochronous cyclotron was focused at the center of a 1.5 m diameter scattering chamber. The beam spot at the center of the target was 2 mm × 2 mm with an angular divergence of 5 mrad. Beam currents ranged from 15 to 100 nA depending on the detector angles.

The outgoing alpha particles were detected by two identical counter telescopes which were mounted coplanar with and on opposite sides of the beam. Each telescope consisted of a 300 μm silicon surface barrier ΔE detector followed by a 4 mm Si(Li) E detector mounted at 45° to provide an effective thickness of 5.65 mm which is sufficient to stop 140 MeV alpha particles. The solid angles subtended by the detectors were 1.35 and 1.39 msr, respectively.

For the ^{9}Be runs a self-supporting foil of 2.52 mg cm^{-2} thickness was used. For the other measurements, high purity ^{16}O, and ethane (C_2H_6) and isotopically enriched ^{20}Ne gases were used in a 12 cm diameter gas cell. The typical pressure was about 1 atmosphere. In order to define the gas target thickness and to prevent particles scattered by the gas cell windows from entering the detector telescopes, a double slit collimator system was used in front of each telescope. The overall angular resolution provided by the slit system was 1.9° and 2.8°, respectively.

Details of the experimental setup are discussed in Ref. 35. Briefly fast timing signals from the ΔE preamplifiers provided start and stop signals for a time-to-amplitude converter in order that real and accidental coincidences could be simultaneously stored. The timing resolution was approximately 3 ns. In addition a slow coincidence was required between the four detectors and the TAC signal. The analog signals from the four detectors and the TAC signal were gated by the slow coincidence and fed to analog-to-digital converters interfaced to an IBM 360/44 computer. Dead time losses were determined using a fourfold pulser unit triggered at a rate proportional to the beam current.

All ADC data were written, event by event, on magnetic tape for off-line reanalysis. In addition a very flexible data handling code permitted online calibration, particle identification, random coincidence subtraction, and one-and two-dimensional array accumulation.

On reanalysis two-dimensional spectra were constructed for the parameters F_3 vs T_1, where T_1 is the total energy deposited in one telescope and $F_3 = T_1 + T_2 + T_3$. Here T_2 is the energy deposited in the second telescope and T_3 the (computed) residual nucleus recoil energy. Clearly $F_3 = T_0 - B$, where T_0 is the incident kinetic energy and B the alpha binding energy in the target. Thus we refer to distributions of the parameter F_3 as "binding energy" spectra. Each F_3 vs T_1 spectrum was gated by the computer generated particle identification functions to correspond to alpha-alpha coincidences and random events were subtracted. The counts in each F_3 vs T_1 spectrum were summed along the kinematic line for each final state in the residual nucleus in bins of $\Delta T_1 = 2.4$ MeV. The resulting spectra were plotted as a function of T_1 yielding the energy sharing cross section $d^3\sigma/d\Omega_1 d\Omega_2 dT_1$.

The errors in the calculated cross sections are predominantly statistical. An error evaluation

TABLE I. Experimental angle pairs θ_1/θ_2 and minimum allowed recoil momenta q_{min}.

Target	θ_1/θ_2	q_{min} (MeV/c)
^{20}Ne	43.71°/−43.71°	0
	49.39°/−38.0°	0
	57.20°/−30.0°	0
	63.82°/−23.0°	0
^{16}O	43.16°/−43.16°	0
	55.97°/−30.0°	0
	63.82°/−23.0°	10
^{12}C	43.11°/−43.11°	0
	49.15°/−37.0°	0
	55.86°/−30.0°	0
	62.21°/−23.0°	0
^{9}Be	44.19°/−44.19°	0
	47.39°/−41.0°	0
	50.38°/−38.0°	0
	54.85°/−33.5°	0
	58.30°/−30.0°	0
	61.25°/−27.0°	0
	64.65°/−23.5°	0
	40.0°/−40.0°	69
	36.0°/−36.0°	125

showed the errors due to other sources such as random subtraction, solid angles, target thickness, gas pressure and temperature, current integrator, slit scattering, dead time correction, and bin size measurements could be neglected relative to the statistical errors.

B. Experimental results

The $(\alpha, 2\alpha)$ reaction yields were measured for ^{20}Ne, ^{16}O, ^{12}C, and ^{9}Be targets at 20 angle pairs with an incident energy $E_\alpha = 140$ MeV. Table I shows the data taken in the experiment, where q_{min} is the allowed minimum recoil momentum of the residual nucleus for the ground state transition. All but three of these angle pairs permit $q_{min} = 0$. At these so-called "quasi-free" angle pairs the reaction can proceed leaving the residual nucleus at rest.

The binding energy spectra for ^{20}Ne, ^{16}O, ^{12}C, and ^{9}Be$(\alpha, 2\alpha)$ reactions at symmetric quasi-free angles are shown in Fig. 1. Each binding energy spectrum shows a prominent isolated peak corresponding to the ground state of the residual nucleus. In the ^{20}Ne$(\alpha, 2\alpha)^{16}$O spectrum, a peak corresponding to the 6.05 and 6.13 MeV doublet of ^{16}O is also rather clear. Other states, due to poor counting statistics, could not be identified. In the ^{16}O$(\alpha, 2\alpha)^{12}$C spectrum, the 2^+(4.43 MeV) peak is comparable in magnitude to that of the ^{12}C(g.s.) transition. In addition, there is some evidence for a broad peak corresponding to the 4^+(14.0 MeV) state. The ground and first excited states of ^{8}Be in ^{12}C$(\alpha, 2\alpha)^{8}$Be are smeared somewhat in the binding energy spectrum. This is largely due to a slight gain shift of the detector telescopes and some nonlinearity of the F_3 functions in the F_3 vs T_1 spectra. However, the two-dimensional F_3 vs T_1 spectrum used to calculate the cross section had a much clearer separation of the two states. For ^{9}Be$(\alpha, 2\alpha)^{5}$He reaction, no ^{5}He state other than the ground state is seen in the binding energy spectrum.

The energy sharing spectrum for the transition leaving the residual nucleus in its ground state was extracted for each target and angular setting. Three additional spectra for ^{20}Ne$(\alpha, 2\alpha)^{16}$O(6 MeV), ^{16}O$(\alpha, 2\alpha)^{12}$C(4.43 MeV), and ^{12}C$(\alpha, 2\alpha)^{8}$Be(2.9 MeV) at the symmetric quasi-free angle pair were also obtained.

The ground state (g.s.) energy sharing spectra for the symmetric quasi-free angle pairs are presented in Fig. 2. There are several systematic

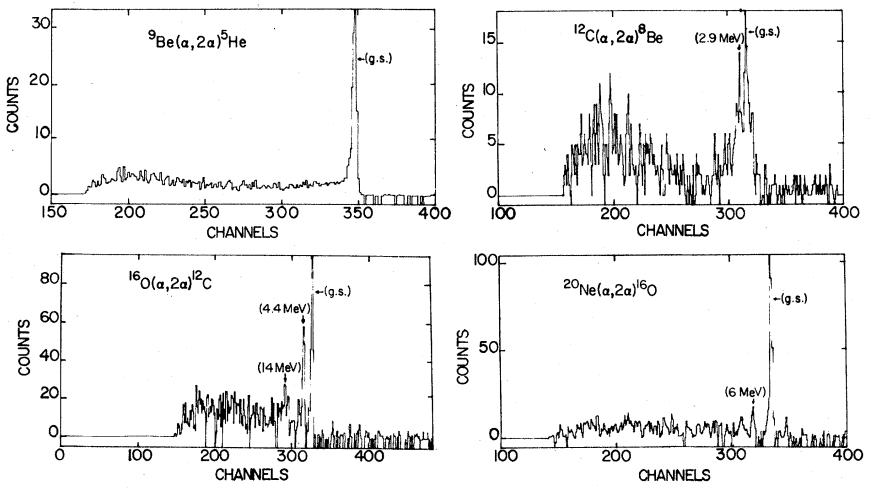

FIG. 1. Binding energy spectra for the $(\alpha, 2\alpha)$ reaction at 140 MeV on ^{9}Be, ^{12}C, ^{16}O, and ^{20}Ne.

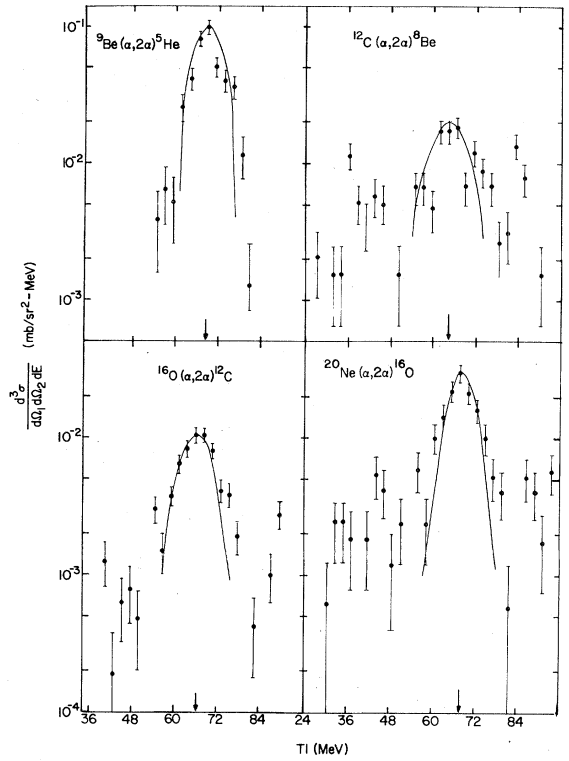

FIG. 2. Energy sharing spectra for the 140 MeV (α, 2α) reaction at symmetric quasi-free angle pairs on ^{9}Be, ^{12}C, ^{16}O, and ^{20}Ne leading to the ground states of the various residual nuclei. The arrows indicate the zero recoil momentum ($P_3 = 0$) points. The solid lines are DWIA predictions.

features which characterize these spectra. Firstly, the maximum in each quasi-free angle pair spectrum comes at the minimum recoil momentum of the residual nucleus. An arrow in each spectrum indicates this point. Secondly, the structure of the spectra is characterized by a broad, smooth bump which is characteristic of the quasi-free knockout mechanism for $L = 0$ transitions.[36] Spectra for nonsymmetric angle pairs, two of which are shown in Fig. 3, are very similar and the full width at the half maximum (FWHM) of the spectrum for each target is essentially independent of the particular angle pair when plotted against the momentum of the recoil nucleus rather than outgoing particle energy. The approximate widths are 70 MeV/c for ^{20}Ne(α, 2α)^{16}O(g.s.), 90 MeV/c for ^{16}O(α, 2α)^{12}C(g.s.), 90 MeV/c for ^{12}C(α, 2α)^{8}Be(g.s.), and 70 MeV/c for ^{9}Be(α, 2α)^{5}He(g.s.).

When one of the detector angles is less than 30° strong contributions from mechanisms other than knockout are evident. For example in Fig. 3 the data for ^{20}Ne(α, 2α) at $\theta_1/\theta_2 = 63.82°/-23°$ show a large yield on the lower energy side of the quasi-

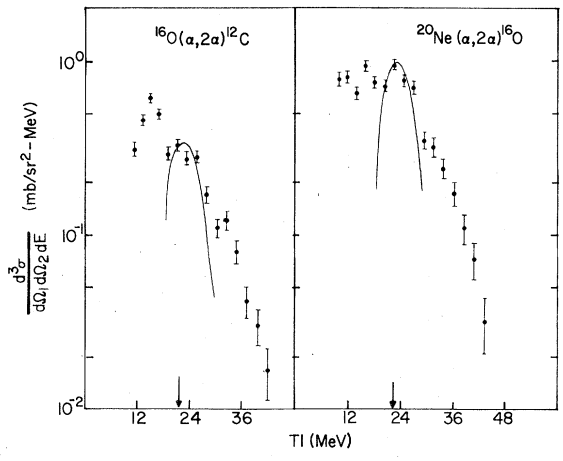

FIG. 3. Energy sharing spectra for ^{16}O(α, 2α)^{12}C (g.s.) and ^{20}Ne(α, 2α)^{16}O(g.s.) at $\theta_1/\theta_2 = 63.8°/-23°$. Arrows indicate minimum recoil momentum points and solid lines are DWIA predictions.

free distribution, although there is no well defined peak. In the same figure the data for ^{16}O show evidence of sequential alpha decay following inelastic scattering to levels in the target nucleus centered around 20 MeV excitation. In this excitation region many alpha decay channels are open and cannot be resolved in the experiment.

III. ANALYSIS

A. DWIA calculations

The theoretical analysis of the data was performed using the distorted wave impulse approximation code written by Chant and Roos.[19] The differential cross section for the reaction $A(\alpha, 2\alpha)B$ for the knockout of an alpha particle with total angular momentum J and orbital angular momentum L is given by

$$\frac{d^3\sigma^{LJ}}{d\Omega_1\, d\Omega_2\, dT_1} = F_K S_{LJ} \frac{d\sigma}{d\Omega}\bigg|_{\alpha\text{-}\alpha} \sum_{\Lambda} |T_{BA}^{\alpha L\Lambda}|^2, \qquad (1)$$

where F_K is a kinematic factor, $d\sigma/d\Omega\,|_{\alpha\text{-}\alpha}$ is the two-body α-α cross section, and S_{LJ} is the cluster spectroscopic factor for specific L and J. The quantity

$$T_{BA}^{\alpha L\Lambda} = \frac{1}{(2L+1)^{1/2}} \int \chi_2^{(-)*}(\vec{r})\chi_1^{(-)*}(\vec{r})\chi_0^{(+)}(\gamma\vec{r}) \times \phi_{L\Lambda}^{\alpha}(\vec{r})\, d\vec{r}, \qquad (2)$$

where the $\chi_i^{(\pm)}$ are distorted waves, $\gamma = B/A$, and $\phi_{L\Lambda}^{\alpha}(\vec{r})$ is the bound state wave function of the alpha cluster in the target nucleus. We refer to this quantity as the "distorted momentum distribution", since in the limit of no distortion $T_{BA}^{\alpha L\Lambda}$ reduces to $\phi_{L\Lambda}^{\alpha}$ in a momentum representation at the point $\vec{q}$

$= -\vec{p}_B$. In practice we shall see that distortion effects are quite severe for the present data.

It is important to note that Eq. (1) employs a factorized impulse approximation in which the two-body cross section enters as a multiplicative factor rather than as a t operator within the integrand of Eq. (2). Thus the integration over what is properly a fully off-energy-shell matrix element is replaced by the half off-shell value at the asymptotic kinematics. Furthermore, in practice we make the additional approximation of replacing $d\sigma/d\Omega\,|_{\alpha\text{-}\alpha}$ by the corresponding quantity determined from a measured (on-shell) two-body cross section. In analyzing $(p, p\alpha)$ data at 100 MeV, Roos *et al.*[17] found little error arose from the neglect of half off-shell effects, although there was some breakdown in the factorization approximation. This problem is investigated for the present data in Sec. III B.

B. Factorization test

In order to test our description of the assumed reaction mechanism we first divided the measured experimental cross sections at $p_B = 0$ by the kinematic factor F_K. According to Eq. (1) we have

$$\frac{d^3\sigma}{d\Omega_1\, d\Omega_2 dT_1}/F_K = [S_\alpha\,|\phi(-\vec{p}_B)|^2]\,\frac{d\sigma}{d\Omega}\bigg|_{\alpha\text{-}\alpha}, \qquad (3)$$

where $|\phi(-\vec{p}_B)|^2 = \sum_\Lambda |T_{BA}^{\alpha L\Lambda}|^2$.

In principle S_α is constant. In addition, explicit DWIA calculations of the quantity $|\phi(-\vec{p}_B)|^2$ varied by less than ±10% at the $p_B = 0$ point over the entire angular range studied for all four targets. Thus, in the factorized DWIA, the ratio constructed in Eq. (3) should be proportional to the two-body cross section $d\sigma/d\Omega\,|_{\alpha\text{-}\alpha}$ to within this accuracy. Results are shown in Fig. 4 for all four targets studied plotted as a function of the two-body c.m. scattering angle. Also shown are measured free α-α cross sections at 120 and 140 MeV lab energy.[37,38] As indicated in Fig. 4, since the struck alpha particle is bound, the effective scattering energy (in the final state) is less than 140 MeV. It is found that, for all four targets, the ratios $(d^3\sigma/d\Omega_1 d\Omega_2 dT_1)/F_K$ can be normalized to lie between the free cross sections at 120 and 140 MeV and that the angular variation of the data points follows the free cross sections very closely over almost three orders of magnitude.

The result of the preceding series of factorization tests with the quasi-free angular distribution data is encouraging. However, there is no free α-α scattering data available at energies between 120 and 140 MeV and the uncertainties in the extracted half-shell cross sections are quite large. In order to choose a suitable energy for the free

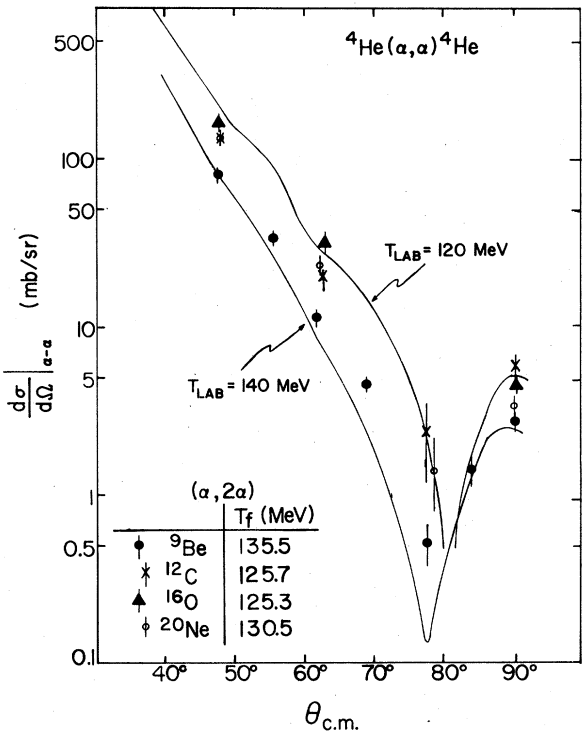

FIG. 4. Half-shell α-α cross sections extracted from 140 MeV $(\alpha, 2\alpha)$ reactions on ^{9}Be, ^{12}C, ^{16}O, and ^{20}Ne. The solid lines represent measured free α-α elastic scattering cross sections at 120 and 140 MeV.

α-α cross section which is used to replace the half-shell cross section, three possible prescriptions were examined. On-shell α-α cross sections were obtained by interpolation at energies: (a) $E = T_f$, (b) $E = \frac{1}{2}(T_f + T_i)$, and (c) $E = T_i$. Using these cross sections the ratio of the experimental three-body cross section at $p_B = 0$ and the product $F_K\, d\sigma/d\Omega$ is compared with the calculated $|\phi(0)|^2$ at each angle for each of the $(\alpha, 2\alpha)$ reactions under investigation. Differences between the three prescriptions are not large. However, a careful comparison of the extracted $|\phi(0)|^2$ obtained from the on-shell cross section at the three different energies with the calculated $|\phi(0)|^2$ shows that the T_f prescription gives slightly better consistency between the experimental and calculated results. This result is in agreement with other investigations and with the result that the final energy prescription arises as the first term of a multiple scattering expansion based on the Faddeev equations.[39] It thus is used throughout the ensuing analyses.

These tests have been carried out with different sets of distorting and bound state parameters. The factorization characteristics are found to be insensitive to the choice of these parameters.

C. Comparison of DWIA calculations with experiment

In order to carry out the DWIA calculations it is necessary to evaluate both the distorted wave functions and the bound cluster "wave function" appearing in the integrand of Eq. (2). The latter quantity, $\phi^{\alpha}_{L\Lambda}(\vec{r})$, more properly represents the result of projecting the target nucleus wave function onto the product of the residual nucleus wave function and the internal wave function of an alpha particle in its ground state. Following common practice in both knockout and transfer reaction analyses we have replaced $\phi^{\alpha}_{L\Lambda}(r)$ in our calculations by an eigenfunction of a Woods-Saxon potential with an energy eigenvalue equal to the alpha particle separation energy. The principal quantum number N is chosen on the basis of conservation of oscillator shell model quanta. Thus

$$2(N-1)+L=\sum_{i=1}^{4}2(n_i-1)+l_i\,, \tag{4}$$

where the n_i and l_i are individual nucleon principal quantum numbers and orbital angular momenta, respectively. Thus, assuming $(1s^4)(1p^n)$ configurations for $A \leq 16$, $L=0(2)$ transitions must have $N=3(2)$. For ^{20}Ne, if we assume an initial $(1s^4)(1p^{12})(2s1d)^4$ configuration, $L=0(2)$ transitions have $N=5(4)$.

Initially calculations were carried out using bound state potential parameters yielding a potential consistent with the known rms radii of the target nuclei. For the ^{16}O target the parameters used are listed in Table II. The values ($R=1.22\times 12^{1/3}$ fm, $a=0.76$ fm) are quite similar to the results of a folding procedure which was used successfully in an earlier analysis[17] of the $(p,p\alpha)$ reaction at 100 MeV. Also listed in Table II are potentials used for the incident and emitted alpha particles. Our notation is such that, for example, C139 is a potential obtained by fitting $\alpha+^{12}$C elastic scattering at a laboratory energy of 139 MeV. Notice that our use of $\alpha+^{12}$C potential parameters is consistent with the formal result[40] that the projectile-ejectile interaction is, in principle, included to all orders via the two-body t matrix.

Using the parameters C139/C139/C139 for the incident/emitted/emitted alpha particles for ^{16}O$(\alpha,2\alpha)^{12}$C(g.s.) at 140 MeV the shapes of the experimental distributions at three different angle pairs were reasonably well reproduced. Typical results are shown in Fig. 2. Somewhat surprisingly, however, the extracted spectroscopic factor S_α was approximately 25, more than 100 times the theoretical value of 0.23 predicted in the Kurath shell model calculations.[22] This result is similar to that obtained by Chant and Roos[19] in their DWIA analysis of the 90 MeV $(\alpha,2\alpha)$ data. Noting that, at $p_B=0$, the emitted alpha particle kinetic energies are each about 66 MeV the sets C139/C104/C104, C104/C104/C104, C139/C56/C56, C139/C56′/C56′ were tried. However, these calculations produced a variation in the spectroscopic factor of less than a factor of 3. Finally, to allow for the energy variation of the emitted alphas in the exit channel (between 40 and 90 MeV) calculations were carried out using the various combinations of potentials listed above with real potential strengths readjusted to yield volume integrals $J/4A$ corrected for an energy dependence of $-1.3\,E_{\text{c.m.}}$, where $E_{\text{c.m.}}$ is the c.m. energy. This is consistent with the observed variation of the real volume integral in the range $30<E<160$ MeV and $4<A<60$. In all cases the extracted spectroscopic factors were at least 30 times larger than the theoretical value.

A similar study[41] by Jain and Sarma of the sensitivity of the spectroscopic factor extracted from the 90 MeV ^{16}O$(\alpha,2\alpha)^{12}$C data[29,30] to the choice of optical parameters has been reported. These authors correctly point out that the optical parameters selected for the original calculations of Chant and Roos[19] are not in good agreement with appropriate elastic scattering data (being in fact obtained from fits to slightly heavier targets). By

TABLE II. Optical potential parameters [a] for ^{16}O$(\alpha,2\alpha)^{12}$C (g.s.) initial calculations.

Set series	V_0 [b]	r_0	a	r_c	W_0	r_0'	a'	Ref.
B.S. [c]	72.5	1.22	0.76	1.24				
C139	108.1	1.22	0.76	1.26	16.9	1.85	0.47	52
C104	114.0	1.22	0.80	1.26	13.8	1.91	0.50	52
C56	151.9	1.24	0.665	1.4	28.05	1.24	0.64	53
C56′	216.8	1.3	0.58	1.4	38.05	1.5	0.32	53

[a] The optical potential is defined to be $V_{\text{opt}}=-V_0 f(r,r_0,a)-iW_0 f(r,r_0',a')+V_c$, where $f(r,r_0,a)=\{1+\exp[(r-r_0A^{1/3})/a]\}^{-1}$, A is the target mass, V_C is the Coulomb potential of a uniform charged sphere of radius $r_cA^{1/3}$.

[b] V_0 and W_0 in MeV: r_0, r_0', a, a', and r_c in fm.

[c] Bound state.

selecting optical parameters from the work of Pehl,[42] Jain and Sarma obtain improved fits to the relevant elastic scattering data and obtained a spectroscopic factor only about five times the theoretical value. We have carried out additional calculations which suggest that this reduction in S_α is a consequence not of the detailed improvements in the elastic scattering fits but rather of the fact that, in his early work, Pehl reported the shallowest potential from among the various discrete ambiguities. Specifically the potential of Ref. 42 has $V = 33$ MeV and $J/4A$ roughly one fourth of the value derived from the energy dependence described above. In the light of more recent work[43] we argue that this choice is unphysical and does not satisfactorily remove the large discrepancy in S_α which we have noted.

Similar problems are encountered for the other targets. Initial calculations reproduced the shapes of the $(\alpha, 2\alpha)$ distributions but gave spectroscopic factors of 9 for ^{9}Be, 11 for ^{12}C, and 27 for ^{20}Ne which are much larger than the theoretical values[22,23] of 0.57, 0.55, and 0.21, respectively. As found for ^{16}O reasonable variations in distorting parameters failed to remove the disagreement between theory and experiment.

Next a test of the sensitivity of the calculations to the bound state parameters was carried out. The results were found to be relatively insensitive to the diffuseness parameter "a" and to the Coulomb radius r_C. Variation of the bound state radius parameter r_0 produced no change in the shape of the energy sharing distribution, but resulted in significant changes in the predicted magnitude. To illustrate this effect we have plotted in Fig. 5 the distorted momentum distribution at $p_B = 0$, $|\phi(0)|^2$, as a function of the bound state radius parameter r_0 for ^{16}O$(\alpha, 2\alpha)^{12}$C(g.s.) at $\theta_1 = -\theta_2 = 43.16°$. In these calculations the distorting parameter set was $C139/C139/C139$. For the bound state, the parameters a and r_C were fixed at 0.76 and 1.3 fm, respectively, while the potential strength was readjusted at each value of r_0 to yield a solution with the empirical alpha separation energy. It is seen that the magnitude of $|\phi(0)|^2$ is increased by a factor of approximately 120 on changing r_0 from 1.2 to 2.52 fm which thus serves to reduce the extracted spectroscopic factor to approximately 0.23, the anticipated value.

It should be noted that the value $r_0 = 2.52$ fm for ^{16}O$(\alpha, 2\alpha)^{12}$C(g.s.) does not lead to noticeable deterioration in the fit to the shape of the energy sharing distribution. However, the associated $3S$ wave function has an rms radius of 4.37 fm while the rms radius of the potential is 3.56 fm. Both values are well in excess of the empirical rms radius of 2.65 fm for ^{16}O. Although the value r_0

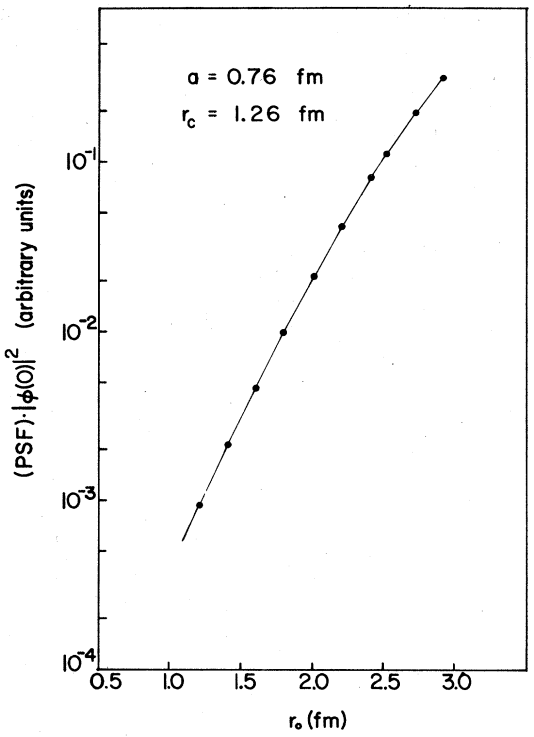

FIG. 5. Dependence of the quantity $|\phi(0)|^2$ on the bound state radius parameter r_0 for ^{16}O$(\alpha, 2\alpha)^{12}$C(g.s.) at $E_\alpha = 140$ MeV. The diffuseness is held fixed at $a = 0.76$ fm and the Coulomb radius parameter is $r_C = 1.26$ fm.

= 2.52 fm is thus clearly excessive, it is important to note that comparable values have been used in analyses of alpha-transfer reactions in order to reproduce the experimental absolute cross sections (that is, to obtain absolute spectroscopic factors in agreement with shell model theories). For example, the authors of Refs. 11 and 12 used bound state well radii of $R = 2.0A_c^{1/3}$ fm and $R = 1.2\,(A_c^{1/3} + 4^{1/3})$ fm, respectively, where A_c is the mass number of the core. These values are equivalent to $r_0 = 2.0$ and 2.05 fm for ^{16}O in our parametrization.

Our decision to characterize the enhanced $(\alpha, 2\alpha)$ cross sections by an increased value of r_0 thus has the merit of consistency with transfer reaction analyses and is clearly preferable to the introduction of unphysical optical potentials in *both* knockout and transfer analyses. Nevertheless, it is a somewhat arbitrary device. We shall return to the question of the implications of this choice in Sec. III F. For the present we choose $r_0 = 2.52$ fm for all targets studied in order to investigate the resultant fits to the energy sharing distributions as well as the deduced spectroscopic factors.

Calculated energy sharing spectra for all four ground state transitions at the symmetric quasi-free angle pair are shown in Fig. 2. The optical parameters used are listed in Table III. It should be noted that, with the exception of ^{9}Be, these are pure $L=0$ transitions. For ^{9}Be, as we have discussed previously,[17] roughly equal admixtures of $3S$ and $2D$ transitions are expected. These terms add incoherently and the curve shown in Fig. 2 is the summed result. As found for $(p,p\alpha)$ at 100 MeV the $2D$ admixture has little effect.

In general agreement between theory and experiment in Fig. 2 is good. Aside from the regions of sequential processes, comparable agreement is also apparent in Fig. 3 in which results are shown for the ground state transitions at asymmetric angle pairs.

D. Spectroscopic factors: ground state transitions

The ground state spectroscopic factors extracted from our 140 MeV data are shown in Table IV together with theoretical values obtained from structure calculations employing shell model[22] and SU_3 model[23] approaches. All data sets have been included with the exception of the ±36° angle pair for ^{9}Be which was poorly reproduced in the DWIA calculations. This difficulty can be attributed to the fact that this angle pair involves much higher momentum components in the alpha wave function than any other angle pair chosen. Specifically, the minimum value of p_B is 125 MeV/c which is to be compared with a distorted momentum distribution width of ±70 MeV/c for ^{9}Be. As a result the knockout cross section is suppressed, and accuracy in treating the bound state and distorted waves becomes more crucial. Also competing reaction mechanisms may play a more significant role.

From Table IV it is seen that the extracted spectroscopic factors for each target vary between ±20% and ±30% over the angular range studied. The uncertainties attached to the average spectroscopic factors quoted are merely standard deviations of the angular variations. Clearly many sources of relative and absolute errors have been ignored.

Agreement between theory and experiment is generally good. Clearly our choice of $r_0=2.52$ fm guarantees this result for ^{16}O. However, it is seen that this choice, made arbitrarily for the other targets, leads to an excellent description of the *relative* strengths for the four targets.

As a further test of our chosen bound state geometry, calculations were carried out for $(\alpha,2\alpha)$ data obtained by other groups at lower energies. Results for the four targets under discussion are compared with our 140 MeV results in Table V. For ^{9}Be$(\alpha,2\alpha)^5$He(g.s.) data at $E_\alpha=55$, 49.2, and 42.8 MeV (Refs. 26 and 27) have been analyzed. It is surprising that at these low energies, where the quasi-free knockout reaction mechanism may be less dominant and the free α-α cross sections oscillate, we obtain an experimental spectroscopic factor consistent with that from 140 MeV data to within about 50%. The results of the same analysis of ^{12}C data at $E_\alpha=90$ MeV (Ref. 29 and 30) and ^{16}O data at 90 MeV (Refs. 29 and 30), 52.5 and 46 MeV

TABLE III. Optical potential parameters [a] for final calculations.

Reaction	System	V_0 [b]	r_0	a	r_c	W_0	r_0'	a'	r_{rms}	$J/4A$	Ref.
^{9}Be$(\alpha,2\alpha)^5$He	$\alpha+^9$Be	72.63	1.36	0.765	1.3	23.8	1.36	0.765		329	54
	$\alpha+^5$He	72.63	1.36	0.765	1.3	23.8	1.36	0.765		396	54
	B.S. [c]	36.69	2.52	0.765	1.3				4.74	806	
^{12}C$(\alpha,2\alpha)^8$Be	$\alpha+^{12}$C	108.1	1.22	0.76	1.26	16.9	1.85	0.47		356	52
	$\alpha+^8$Be	108.1	1.22	0.76	1.26	16.9	1.85	0.47		402	52
	B.S.	35.80 38.51 [d]	2.52	0.655	1.26				4.03	700	
^{16}O$(\alpha,2\alpha)^{12}$C	$\alpha+^{16}$O	108.1	1.22	0.76	1.26	16.9	1.85	0.47		330	52
	$\alpha+^{12}$C	108.1	1.22	0.76	1.26	16.9	1.85	0.47		356	52
	B.S.	30.50 35.13 [d]	2.52	0.7825	1.26				4.37	604	
^{20}Ne$(\alpha,2\alpha)^{16}$O	$\alpha+^{20}$Ne	110.6	1.22	0.82	1.3	17.9	1.77	0.63		338	55
	$\alpha+^{16}$O	110.6	1.22	0.82	1.3	17.9	1.77	0.63		358	55
	B.S.	46.34	2.52	0.78	1.3				5.44	892	

[a] The optical potential is defined to be $V_{opt}=-V_0 f(r,r_0,a)-iW_0 f(r,r_0',a')+V_C$, where $f(r,r_0,a)=[1+\exp\{(r-r_0A^{1/3})/a\}]^{-1}$; A is the target mass; V_C is the Coulomb potential of a uniform sphere of radius $r_cA^{1/3}$.

[b] V_0 and W_0 in MeV, r_0, r_0', a, a', r_C, and r_{rms} in fm, $J/4A$ in MeV fm^3.

[c] Bound state.

[d] When the core is left in its first excited state.

TABLE IV. Spectroscopic factors for angle pairs (θ_1/θ_2) extracted by means of the DWIA analysis. The average $\langle S_\alpha^{exp}\rangle$ is a statistical average of all angle pairs.

Reaction	θ_1/θ_2	S_α^{exp}	$\langle S_\alpha^{exp}\rangle$	S_α^{theory}	Ref.
$^{9}Be(\alpha, 2\alpha)^{5}He(g.s.)$	44.19°/−44.19°	0.656			
	47.39°/−41.0°	0.930			
	50.38°/−38.0°	0.574		0.57	22
	54.85°/−33.5°	0.635			
	58.39°/−30.0°	0.579	0.633 ± 0.120		
	61.25°/−27.0°	0.622			
	64.65°/−23.5°	0.540			
	40.0°/−40.0°	0.527			
$^{12}C(\alpha, 2\alpha)^{8}Be(g.s.)$	43.11°/−43.11°	0.641		0.674	47
	49.15°/−37.0°	0.682		0.55	22
	55.86°/−30.0°	0.421	0.558 ± 0.107	0.285	23
	62.21°/−23.0°	0.487		0.759	56
				0.675	56
$^{16}O(\alpha, 2\alpha)^{12}C(g.s.)$	43.16°/−43.16°	0.209		0.295	47
	55.97°/−30.0°	0.304		0.23	22
	63.82°/−23.0°	0.222	0.244 ± 0.046	0.296	23
				0.333	56
				0.296	56
$^{20}Ne(\alpha, 2\alpha)^{16}O(g.s.)$	43.71°/−43.71°	0.157			
	49.39°/−38.0°	0.235		0.21	23
	57.20°/−30.0°	0.220	0.202 ± 0.029	0.182	47
	63.82°/−23.0°	0.196			
$^{12}C(\alpha, 2\alpha)^{8}Be(2.9\ MeV)$	43.16°/−43.16°	1.74	1.74	0.72	22
				0.592	23
$^{16}O(\alpha, 2\alpha)^{12}C(4.43\ MeV)$	43.11°/−43.11	1.26	1.26	1.31	22
				1.48	23

(Refs. 26 and 27) and ^{20}Ne data at 78 MeV (Ref. 28) are also shown in Table V. The results from the ^{12}C and ^{16}O data at 90 MeV are consistent with the results from our own data to within a factor of 3. For the ^{16}O data at around 50 MeV the agreement is within a factor of 4. For ^{20}Ne at 78 MeV agreement with our 140 MeV result is within the experimental error. Considering the original disagreement of over a factor of 100, these differences are not large.

The optical model parameters used for the lower energy calculations are the same as those listed in Table III. We have not investigated the sensitivity of the lower energy results to the choice of distorting potentials. Clearly there are large uncertainties and a more consistent description might be possible. An important ingredient of any improved analysis would be a more systematic treatment of the energy dependence of the alpha optical potential.

E. Transitions to the first excited states of ^{8}Be and ^{12}C

The overlaps of $^{12}C \rightarrow \alpha + {}^{8}Be$ (2.9 MeV, 2^+) and $^{16}O \rightarrow \alpha + {}^{12}C$ (4.43 MeV, 2^+) have also been investigated with the quasi-free knockout reactions $^{12}C(\alpha, 2\alpha)^{8}Be$ (2.9 MeV) and $^{16}O(\alpha, 2\alpha)^{12}C$(4.43 MeV) at angles 43.11°/−43.11° and 43.16°/−43.16°,

TABLE V. Spectroscopic factors S_α^{exp} extracted by means of the DWIA analysis at symmetric quasi-free angle pairs.

Reactions	E_α (MeV)	S_α^{exp}	$\langle S^{exp}\rangle E_\alpha = 140$ MeV
$^{9}Be(\alpha, 2\alpha)^{5}He(g.s.)$	55	0.820 ± 0.082	
	49.2	0.655 ± 0.068	0.633
	42.8	0.936 ± 0.156	
$^{12}C(\alpha, 2\alpha)^{8}Be(g.s.)$	90	0.196 ± 0.014	0.558
$^{16}O(\alpha, 2\alpha)^{12}C(g.s.)$	90	0.0942 ± 0.011	
	52.5	0.982 ± 0.225	0.244
	46	0.687 ± 0.125	
$^{20}Ne(\alpha, 2\alpha)^{16}O(g.s.)$	78.6	0.149 ± 0.017	0.202

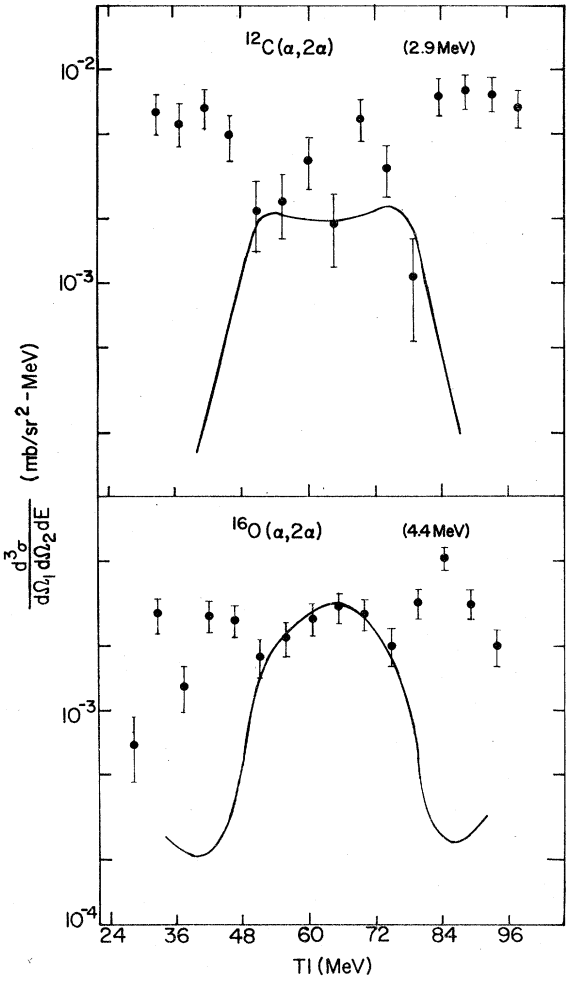

FIG. 6. Energy sharing spectra for $^{12}C(\alpha,2\alpha)^8Be$ (2.9 MeV) and $^{16}O(\alpha,2\alpha)^{12}C$ (4.43 MeV) at $\theta_1/\theta_2 \approx 43°/-43°$. The solid lines are DWIA predictions.

respectively. The measured energy sharing spectra are shown in Fig. 6. The distorting parameters and bound state radius and diffuseness parameters for the DWIA analysis are the same as those for the ground state transitions. Both states have spin and parity 2^+. The principal quantum number $N = 2$ and orbital angular momentum quantum number $L = 2$ are used for the analyses in both cases. The calculated energy sharing distributions can roughly reproduce the experimental data in the region where the two outgoing alpha particle energies are not very different. However, the overall fits are disappointing.

Alpha spectroscopic factors were extracted by comparing the data with the DWIA calculations near the minimum recoil momentum regions. The results are compared with theoretical estimates obtained using a $1p$ shell model[22] and by considering the nuclei as alpha chains,[23] in Table IV. The consistency between the experimental and theoretical values for the $^{16}O \rightarrow \alpha + ^{12}C(4.43\ MeV)$ transition is remarkable while for the $^{12}C \rightarrow \alpha + ^8Be$ (2.9 MeV) transition agreement is within a factor of 3. A difficulty in this case is the possibility of $L = 0$ contributions to the transition which are permitted owing to the unbound nature of the final state and which may be present in $(p,p\alpha)$ data for the same transition.[17] Clearly data with improved statistics coupled with further reaction mechanism studies for the excited states are needed.

F. The alpha cluster bound state wave function

In the preceding sections we have seen that DWIA calculations for the $(\alpha,2\alpha)$ reaction at 140 MeV are relatively insensitive to reasonable changes in the distorting potentials but are strongly dependent on the choice of bound state wave functions $\phi^{\alpha}_{L\Lambda}(\vec{r})$. Specifically, if we accept the theoretical absolute spectroscopic factors quoted as being correct to better than an order of magnitude, calculations using a bound state radius parameter $r_0 \sim 1.22$ fm seriously underestimate the observed absolute cross section. Such a choice for r_0 is "reasonable" in that the resultant wave function and potential have rms radii similar to the empirical target rms radii. However, in order to reproduce the observed cross sections the apparently excessive value of $r_0 = 2.52$ fm is needed. This choice leads to reasonable predicted absolute cross sections for all four targets at 140 MeV without deterioration in the fits to the shapes of the distributions. In addition, consistent absolute cross sections are obtained at lower energies (at least to within a factor of 2–3).

This behavior is in marked contrast to studies[17] of $(p,p\alpha)$ and (p,d^3He) reactions at 100 MeV on ^9Be and ^{12}C and in more recent studies[44,45] at the same energy on ^{16}O and ^{20}Ne. These authors used values of $r_0 \sim 1.1$–1.3 fm which is close to a folding model geometry and thus quite different from our value of $r_0 = 2.52$ fm. However, as pointed out elsewhere[46] the predicted distorted momentum distributions for these $(p,p\alpha)$ transitions are not very sensitive to the radius parameter of the alpha-core bound state. Thus in Ref. 46 we noted that S_α for $^{16}O(p,p\alpha)^{12}C(g.s.)$ at 100 MeV changes by less than a factor of 2 when r_0 is changed from 1.09 to 2.3 fm.

Some of these features can be understood in terms of the radial localization of these reactions. By integrating $T^{\alpha L\Lambda}_{BA}$ of Eq. (2), from r to infinity one obtains a calculated differential cross section $\sigma(r)$, which is a measure of the contribution to the reaction in the range from r to infinity. The difference $\Delta\sigma = \sigma(r) - \sigma(r+\Delta r)$ is thus a measure of

the contribution to the reaction in the range from r to $r+\Delta r$. From a histogram of these differences against r one can investigate the reaction contribution from different values of r. Figure 7 shows the histogram for $^{16}O(\alpha, 2\alpha)^{12}C$(g.s.) at $\theta_1/\theta_2 = 43.16°/-43.16°$, $p_B = 0$, and $E_\alpha = 140$ MeV. For the case of bound state radius parameter $r_0 = 1.22$ fm, one observes a dramatic interference near the region $r \sim r_0 A_c^{1/3}$. It is this calculation which seriously underestimates the experimental absolute cross section. Also shown in Fig. 7 is the corresponding histogram for $r_0 = 2.52$ fm, which leads to agreement with experiment. It is seen that the reaction is now localized to a region near 6.5 fm and that the interference region has been eliminated. At the lower end of Fig. 7 is the corresponding diagram for $^{16}O(p, p\alpha)^{12}C$(g.s.) at 100 MeV using $r_0 = 1.3$ fm and $a = 0.65$ fm. These parameters lead to calculations in good agreement with experiment.[44] Here we see that the reaction is no longer localized in the extreme tail of the bound state wave function, and it is this feature which accounts for the more modest sensitivity to r_0.

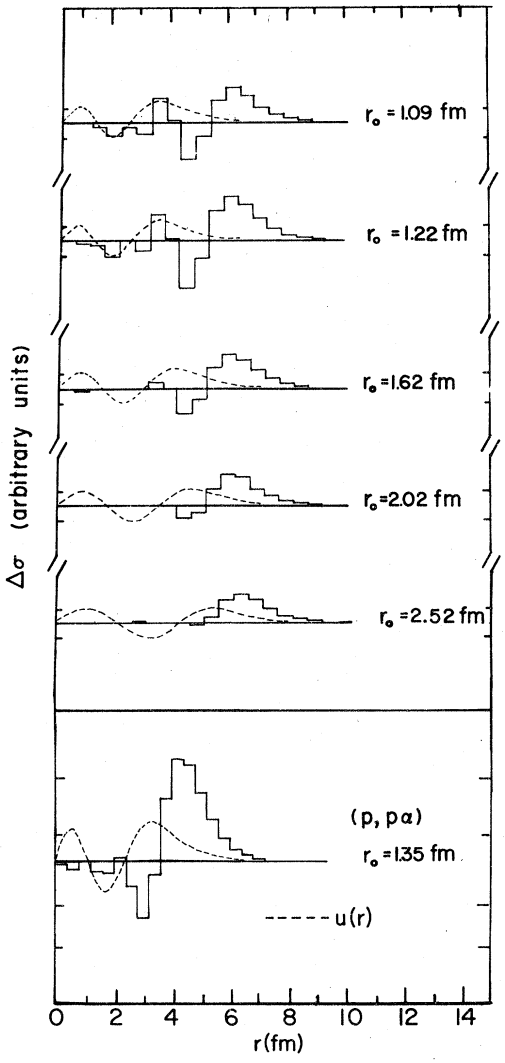

FIG. 7. Histograms of $\Delta\sigma$, the calculated contributions as a function of radius to the $^{16}O(\alpha, 2\alpha)^{12}C$(g.s.) cross section at 140 MeV at $\theta_1/\theta_2 = 43.2°/-43.2°$. Shown are calculations for various values of r_0, the bound state radius parameters. Also shown is a histogram for $^{16}O(p, p\alpha)^{12}C$(g.s.) at 100 MeV for $r_0 = 1.3$ fm. In each case the broken curve is the corresponding bound state radial wave function $u(r)$.

As mentioned briefly in Sec. IIIC our choice of $r_0 = 2.52$ fm is not inconsistent with the values used in alpha transfer reactions. Firstly the $(\alpha, {}^8Be)$ reaction study of Ref. 11 obtained absolute alpha spectroscopic factors for eight $1p$ shell nuclei using an alpha core bound state radius parameter $r_0 = 2.0$ fm. Secondly, the analysis of the $^{12}C(^{16}O, {}^{20}Ne)^8Be$ reaction data[12] used an α-^{16}O bound state radius $R = 1.2(16^{1/3} + 4^{1/3})$ fm, which corresponds to $r_0 = 1.96$ fm in our notation, to reproduce the experimental data. Thirdly, in analyzing the $^{16}O(d, {}^6Li)^{12}C$ reaction Nagel and Koshel[14] were obliged to use a bound state radius $R = 1.27$ $(12^{1/3} + 4^{1/3})$ fm (which corresponds to $r_0 = 2.15$ fm in our notation) in order to reproduce the magnitude of the experimental cross section. These authors pointed out that the magnitude of the calculated cross section increased by a factor of 18 when the bound state radius changed from $1.25 \times 12^{1/3}$ fm to the above value. This is to be compared with a factor of about 24 for a corresponding change in our $^{16}O(\alpha, 2\alpha)^{12}C$(g.s.) analysis. Finally, two groups[47,48] have investigated the $({}^3He, {}^7Be)$ reaction on $1p$ and $2s1d$ shell nuclei and extracted relative alpha spectroscopic factors. The authors of Ref. 47 used $r_0 = 1.2$ fm for $^7Be \rightarrow {}^3He + \alpha$ while Audi *et al.*[48] used a bound state radius $R = 1.25$ $(A_c^{1/3} + 4^{1/3})$ fm. The results of Audi *et al.* are more consistent with the spectroscopic factors obtained in SU_3.

We have seen that while reasonable bound state geometry parameters work well for $(p, p\alpha)$, most alpha transfer analyses and the $(\alpha, 2\alpha)$ reaction at 140 MeV incident energy or less require bound state wave functions enhanced in the nuclear surface by up to an order of magnitude. The device we have selected to achieve this end, namely an increase in r_0, probably has no intrinsic significance. For example, as an alternative, we could have arbitrarily reduced the calculated cluster binding energy.

Yet another approach is that suggested by Jain,[49] who was able to reproduce both the shapes and absolute magnitudes of the 90 MeV data of Ref. 30 using a strong absorption model with a radius pa-

rameter $R = 1.15(A^{1/3} + 4^{1/3})$ fm where A is the target mass number. Unfortunately the success of the strong absorption model calculations does not greatly clarify the situation and more physical explanations for the apparent enhancement of $\phi^{\alpha}_{L\Lambda}(r)$ are needed.

IV. DISCUSSION AND CONCLUSIONS

The present $(\alpha, 2\alpha)$ data suggest the dominance of the quasi-free knockout mechanism. The energy sharing data are well described by the DWIA calculations. Perhaps more importantly the angular dependence of the three-body cross section is in excellent agreement with that obtained in free $\alpha + \alpha$ scattering. However, in spite of consistency with alpha transfer analyses, the necessity of using bound state radii yielding rms radii significantly in excess of those expected is disturbing. Two possible explanations are suggested.

First one might conclude that surface clustering exists in excess of that predicted by the simple shell model calculations considered so far. To examine this question we have considered the treatment of the ^{16}O ground state by Brown and Green,[50] who include 2p-2h and 4p-4h admixtures. We expect an increased yield over our 0p-0h calculation, since these components lead to 4S and 5S bound state wave functions, respectively. Using the amplitudes of Brown and Green we obtain an enhancement in the DWIA cross section of only a factor of 3.5. In fact, any combination of the various components is insufficient to explain the present data using a bound state radius near $r_0 \simeq 1.2$ fm.

Thus more pronounced correlation effects than included in the calculations of Ref. 50 seem to be implied by the present data. However, this result is not at variance with the general success of structure calculations such as Ref. 50. Referring to Fig. 7 we see that nuclear radii of 6 to 7 fm appear to be responsible for the $(\alpha, 2\alpha)$ yield. In this region for the targets studied, nuclear densities are well below 1% of central density and it is only here that alpha clustering of order 100 times shell model estimates are implied by the data. In this regard it is of interest to compare the present results with charge distributions obtained in model independent analyses of electron scattering data. Using the bound alpha cluster wave function obtained with $r_0 = 2.52$ fm we can estimate the charge densities at $r = 6$–7 fm implied by the $(\alpha, 2\alpha)$ data. These are clearly crude estimates. However, it is interesting to note that the results are comparable to (or even exceed) values obtained from electron scattering. For example, for ^{12}C at $r = 7$ fm, Sick[51] obtained $\rho(r)/\rho(0) \sim 2.5 \times 10^{-4}$ from analysis of low momentum transfer electron scattering data whereas our ^{12}C$(\alpha, 2\alpha)^8$Be result is $\rho(r)/\rho(0) \sim 3.5 \times 10^{-4}$. Thus the $(\alpha, 2\alpha)$ data seem to imply that most of the nuclear matter at these very low densities has coalesced into alpha clusters.

As an alternative explanation of the present results we can consider alpha clustering in the surface region *induced* by the projectile. This would correspond to inelastic scattering to states with large alpha parentage followed by knockout. This is an appealing possibility since there exist (at least in ^{16}O) states near the alpha threshold[46] strongly excited in inelastic scattering. Thus, the second step would consist of knocking out an alpha particle weakly bound to the residual nucleus (and therefore having a large asymptotic tail). Unfortunately, no calculations for such processes exist at present. It is worth noting that not only is it necessary to fit the energy sharing distribution, both in shape and magnitude but also such calculations must reproduce the angular dependence of the $(\alpha, 2\alpha)$ cross section. As we have seen this is in excellent agreement with free $\alpha + \alpha$ scattering and thus seems to imply a one-step process. This feature of our data may well prove decisive since one might speculate that dominance of two-step processes would lead to some broadening of the angular distribution. Lastly, similar levels must exist in all four nuclei studied despite their rather different nuclear structure, since all show the same basic effect. Notice also that such calculations must reproduce the alpha transfer data, since similar bound state geometries are needed in those analyses.

ACKNOWLEDGMENTS

We are indebted to the operators and staff of the University of Maryland Cyclotron for their assistance in obtaining stable and reproducible beams. Calculations were carried out using the facilities of the University of Maryland Computer Science Center. Provision of time is gratefully acknowledged. This research was supported in part by the National Science Foundation.

*Present address: Tsing Hua University, Taiwan, R. O. C.
[1]O. Chamberlain and E. Segrè, Phys. Rev. 87, 81 (1952).
[2]J. M. Wilcox and B. J. Moyer, Phys. Rev. 99, 875 (1955).
[3]H. Tyrén, P. Hillman, and Th. A. J. Maris, Nuovo Cimento 6, 1507 (1957); Nucl. Phys. 7, 1 (1958); 7, 10 (1958); Phys. Rev. Lett. 5, 107 (1960).
[4]M. Riou, Rev. Mod. Phys. 37, 375 (1965).
[5]I. E. McCarthy, Rev. Mod. Phys. 37, 388 (1965).
[6]G. Jacob and Th. A. J. Maris, Rev. Mod. Phys. 38, 121 (1966); 45, 6 (1973).
[7]J. D. Cossairt *et al.*, Nucl. Phys. A261, 373 (1976).
[8]D. J. Pisano and P. D. Parker, Phys. Rev. C 14, 475 (1976).
[9]M. E. Cobern, D. J. Pisano, and P. D. Parker, Phys. Rev. C 14, 491 (1976).
[10]N. Anantaraman *et al.*, Phys. Rev. Lett. 35, 1131 (1975).
[11]G. J. Wozniak, D. P. Stahel, J. Cerney, and N. A. Jelley, Phys. Rev. C 14, 815 (1976).
[12]H. Yoshida, Phys. Lett. 47B, 411 (1973).
[13]K. Bethge, Annu. Rev. Nucl. Sci. 20, 255 (1970).
[14]P. Nagel and R. D. Koshel, Phys. Rev. C 14, 1667 (1976).
[15]A. N. James and H. G. Pugh, Nucl. Phys. 42, 441 (1963).
[16]B. Gottschalk and S. L. Kannenberg, Phys. Rev. C 2, 24 (1970).
[17]P. G. Roos *et al.*, Phys. Rev. C 15, 69 (1977).
[18]A. A. Cowley *et al.*, Phys. Rev. C 15, 1650 (1977).
[19]N. S. Chant and P. G. Roos, Phys. Rev. C 15, 57 (1977).
[20]N. S. Chant and P. G. Roos, in *Proceedings of the Second International Conference on Clustering Phenomena in Nuclei, College Park, Maryland, 1975,* edited by D. A. Goldberg, J. B. Marion, and S. J. Wallace (ERDA Technical Information Center, Oak Ridge, Tennessee).
[21]P. G. Roos and N. S. Chant, in *Proceedings of the Second International Conference on Clustering Phenomena in Nuclei, College Park, Maryland, 1975,* edited by D. A. Goldberg, J. B. Marion, and S. J. Wallace (ERDA Technical Information Center, Oak Ridge, Tennessee).
[22]D. Kurath, Phys. Rev. C 7, 1390 (1973).
[23]M. Ichimura, A. Arima, E. C. Halbert, and T. Terasawa, Nucl. Phys. A204, 225 (1973).
[24]J. W. Watson *et al.*, Nucl. Phys. A172, 513 (1971).
[25]M. Jain, P. G. Roos, H. G. Pugh, and H. D. Holmgren, Nucl. Phys. A153, 49 (1970); H. G. Pugh *et al.*, Phys. Rev. Lett. 22, 408 (1969).
[26]A. Guichard *et al.*, Phys. Rev. C 4, 700 (1971).
[27]P. Gaillard *et al.*, Phys. Rev. Lett. 25, 593 (1970).
[28]M. B. Epstein, D. J. Margaziotis, N. S. P. King, and T. A. Cahill, Phys. Rev. C 9, 581 (1974).
[29]J. D. Sherman, Ph.D. thesis, University of California, Berkeley, 1973 (Report No. LBL-1690).
[30]J. D. Sherman, D. L. Hendrie, and M. S. Zisman, Phys. Rev C 13, 20 (1976).
[31]N. Chirapatpimol *et al.*, Nucl. Phys. A264, 379 (1976).
[32]I. E. McCarthy and D. L. Pursey, Phys. Rev. 122, 578 (1961).
[33]A. W. Parker, J. S. Allen, R. L. Yerke, and V. G. Scotland, Phys. Rev. 7, 1093 (1968).
[34]M. Epstein *et al.*, Phys. Rev. 178, 1698 (1969).
[35]C. W. Wang, Ph.D. thesis, University of Maryland, 1978 (unpublished).
[36]H. D. Holmgren, in *Proceedings of the International Conference on Clustering Phenomena in Nuclei, Bochum, Germany, 1969* (International Atomic Energy Agency, Vienna, Austria, 1969).
[37]A. Nadasen *et al.*, Phys. Rev. C 18, 2792 (1978); P. Frisbee, Ph.D. thesis, University of Maryland, 1972 (unpublished).
[38]P. Darriulat, G. Igo, H. G. Pugh, and H. D. Holmgren, Phys. Rev. 137, B315 (1965).
[39]E. F. Redish, G. J. Stephenson, Jr., and G. M. Lerner, Phys. Rev. C 2, 1665 (1970).
[40]D. F. Jackson and T. Berggren, Nucl. Phys. 62, 353 (1965).
[41]A. K. Jain and N. Sarma, *Clustering Aspects of Nuclear Structure and Nuclear Reactions*, edited by W. T. H. Van Oers, J. P. Svenne, J. S. C. McKee, and W. R. Falk (AIP, New York, 1978), p. 568.
[42]R. H. Pehl, Ph.D. thesis, Report No. UCRL 10993, 1963 (unpublished).
[43]See for example D. A. Goldberg and S. M. Smith, Phys. Rev. Lett. 33, 715 (1974); P. Gaillard *et al.*, Nucl. Phys. A131, 353 (1969).
[44]T. A. Carey, Ph.D. thesis, University of Maryland, 1979 (unpublished).
[45]N. S. Chant, *Clustering Aspects of Nuclear Structure and Nuclear Reactions*, edited by W. T H. Van Oers, J. P. Svenne, J. S. C. McKee, and W. R. Falk (AIP, New York, 1978), p. 415.
[46]N. S. Chant, P. G. Roos, and C. W. Wang, Phys. Rev. C 17, 8 (1978).
[47]C. Détraz, H. H. Duhm, and H. Hagner, Nucl. Phys. A147, 488 (1970).
[48]G. Audi, C. Détraz, M. Langevin, and F. Pougheon, Nucl. Phys. A237, 300 (1975).
[49]B. K. Jain, Nucl. Phys. A314, 51 (1979).
[50]G. E. Brown and A. M. Green, Nucl. Phys. 75, 401 (1966).
[51]I. Sick, Nucl. Phys. A218, 509 (1974).
[52]S. M. Smith *et al.*, Nucl. Phys. A207, 273 (1973).
[53]P. Gaillard *et al.*, Nucl. Phys. A131, 353 (1969).
[54]S. Matsuki *et al.*, J. Phys. Soc. Jpn. 26, 1344 (1969).
[55]H. Rebel *et al.*, Nucl. Phys. A182, 145 (1972).
[56]H. H. Gutbrod, H. Yoshida, and R. Bock, Nucl. Phys. A165, 240 (1971); P. Beregi, N. S. Zelenskaja, V. N. Neudatchin, and Yu. F. Smirnov, Nucl. Phys. 66, 513 (1965).